

HYBRID OPTIMAL THEORY AND PREDICTIVE CONTROL FOR POWER MANAGEMENT IN HYBRID ELECTRIC VEHICLE

Kasemsak Uthaichana, Raymond DeCarlo, Sorin Benghea, Miloš Žefran, and Steve Pekarek

Abstract. This paper presents a nonlinear-model based hybrid optimal control technique to compute a suboptimal power-split strategy for power/energy management in a parallel hybrid electric vehicle (PHEV). The power-split strategy is obtained as model predictive control solution to the power management control problem (PMCP) of the PHEV, i.e., to decide upon the power distribution among the internal combustion engine, an electric drive, and other subsystems. A hierarchical control structure of the hybrid vehicle, i.e., supervisory level and local or subsystem level is assumed in this study. The PMCP consists of a dynamical nonlinear model, and a performance index, both of which are formulated for power flows at the supervisory level. The model is described as a bi-modal switched system, consistent with the operating mode of the electric ED. The performance index prescribing the desired behavior penalizes vehicle tracking errors, fuel consumption, and frictional losses, as well as sustaining the battery state of charge (SOC). The power-split strategy is obtained by first creating the embedded optimal control problem (EOCP) from the original bi-modal switched system model with the performance index. Direct collocation is applied to transform the problem into a nonlinear programming problem. A nonlinear predictive control technique (NMPC) in conjunction with a sequential quadratic programming solver is used to compute suboptimal numerical solutions to the PMCP. Methods for approximating the numerical solution to the EOCP with trajectories of the original bi-modal PHEV are also presented in this paper. The usefulness of the approach is illustrated via simulation results on several case studies.

Keywords. Hybrid Optimal Control, Nonlinear Model Predictive Control, Hybrid Electric Vehicles, Power management, Nonlinear Modeling

I. INTRODUCTION

In a hybrid propulsion system, power distribution from two or more energy sources/storages coordinate to deliver the performances demanded by the drivers while considering fuel efficiency and operational constraints. In a parallel hybrid electric vehicle (PHEV), the power demand can be delivered by the main power converter and/or the energy-storage device. Such energy storage devices could be batteries with or without supercapacitors [1], [2]. Examples of main power converters are internal combustion engines (ICEs), fuel cells [3]–[7], etc. In any case, as illustrated in [8]–[11], the power distribution among the main PHEV subsystems is computed at the supervisory level. The model of the PHEV at the supervisory level in this investigation is represented as a bi-modal switched system, as opposed to models with higher number of modes.

Kasemsak Uthaichana is with Department of Electrical Engineering, Chiang Mai University, Chiang Mai, Thailand, (e-mail: kasemsak@chiangmai.ac.th). He is supported by grant Thailand Research Fund, Commission on Higher Education.

Raymond DeCarlo and Steve Pekarek are with School of Electrical and Computer Engineering, Purdue University, West Lafayette, Indiana, USA (email: decarlo@ecn.purdue.edu, pekarek@purdue.edu)

Sorin Benghea is with Control Systems Group, Research Center, United Technologies, East Hartford, Connecticut, USA (email: sbenghea@ieee.org)

Miloš Žefran is with Department of Electrical and Computer Engineering, University of Illinois at Chicago, Chicago, Illinois, USA (email: mze-fran@uic.edu)

The description of the PMCP for constructing the model-based control strategies consists of the PHEV dynamical model, and a performance index (PI), both of which are formulated at the supervisory level. Approaches to solve the PMCP in the literatures can be categorized according to computational requirements as the real-time implementable type, and the global optimal type. The dynamic programming (DP) approaches compute optimal solutions over the driving cycles [8], [9], [12]. The curse of dimensionality of DP is well known. Thanks to recent advances in optimization, approximation approaches have been developed and alleviate this problem [13]–[15]. Since full knowledge of the driving cycles is still required, control using DP is not real-time implementable. Nevertheless, the results can be used as benchmarks for comparing the degree of optimality under replicated driving conditions.

Real-time implementable control strategies for the HEV, not optimal over driving cycles, usually undergo fine-tuning on the actual vehicles for desired performances under various assumptions and driving conditions. The list includes but is not limited to classical instantaneous/static optimization, adaptive equivalent fuel consumption minimization strategy (A-ECMS) [10], simplified rule based, fuzzy logic based [1], [16], [17], and neural network based [4].

The Nonlinear Model Predictive Control (NMPC) technique can provide suboptimal solutions with respect to the PI over the predictive-window. The degree of the optimality of the NMPC strategy is bounded by the instantaneous and the global optimizations. Note that the NMPC still requires a few predictive partitions within the optimization window (preview) of the driving profile, but not as extensively as the dynamic programming approach. The problem underlying the NMPC strategy for PMCP in [18] is a mixed integer optimization problem, e.g., [19], which is computationally expensive.

In this study, the embedding technique in [20] is adopted to formulate the PMCP as a (convex) embedded optimal control problem, EOCP, from the original (non-convex) switched optimal control problem, SOCP. Hence, the degree of complexity for the embedded version of the NMPC problem is lower.

Numerical methods for solving optimization problems include single shooting, multiple-shooting and direct collocation [21]–[24], etc. Difficulties with the single shooting method for the bi-modal PHEV is illustrated in [25]. Therein the necessary conditions are used to solve for the optimal controls. A superior version, called multiple shooting method, is adopted to solve an optimization problem in [26]. Instead of dealing with adjoint equations as in the multiple-shooting method, the direct collocation is adopted in this investigation. The embedding technique in conjunction with the direct collocation method is used to transform the problem into an NLP. The numerical solution to the NLP is computed using sequential quadratic programming (SQP) over a predictive window. More

details on other methodologies to obtain solutions to NMPC problems can be found in [27], [28].

The following describes the paper organization. Section 2 summarizes bi-modal switched model for the PHEV. The performance index is detailed in Section 3. The PMCP is formulated as a multi-objective embedded optimal control problem at the supervisory level in Section 4. Section 5 reviews the embedding technique and presents sufficient conditions for existence of optimal solutions. Section 6 describes the numerical methodology. Section 7 presents the hybrid optimal and NMPC solutions for a sawtooth driving profile, and NMPC solutions for the EPA highway and US06 supplemental FTP (EPA high-speed) driving profiles.

II. PHEV AS A BI-MODAL SWITCHED SYSTEM

The computation at the supervisory level is done based on the presumption that the desired power level can be implemented at the subsystem level. The local closed loop controllers must track the corresponding reference power demand, thereby decoupling the supervisory and local level control problems. Hence, the modeling at the supervisory level should reflect the closed loop behaviors of the subsystems.

A. Summary of Hardware Descriptions

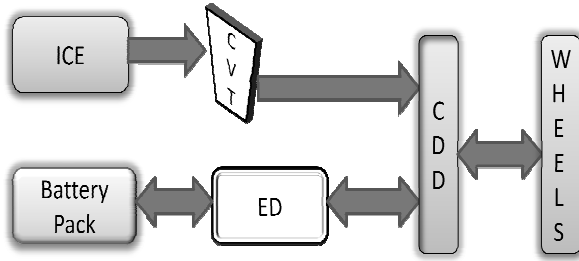


Fig. 1. Power flow diagram of PHEV in this study

The main power source is the 1.9 L ICE, coupled to the driveshaft through a continuously variable transmission (CVT) and clutch in the post-transmission configuration. Thirty 13Ah 12V, lead-acid batteries in series are interfaced with a 30 kW induction ED. Hotel loads are handled by a traditional engine-based charging system. The coupling device and differential (CDD) acts as a summing junction for redirecting the power flow among the ICE-CVT, battery-ED, and the wheels. Figure 1 illustrates power distributions among the main subsystems.

B. Modes of Operation

In [9], five modes of operation describe the essential behavior of the PHEV. Since the PMCP complexity increases exponentially with increased numbers of modes [29], [30], an effort is put forth in this investigation to reduce the number of modes at the supervisory level.

Through careful consideration of the dynamics in each mode of operation, the essential behavior can be approximated using only two modes. As a preview, the mode reduction concept from five to two is illustrated via the numerical results obtained

in this study in Fig. 2. In Fig. 2, $P_{ED} + P_{ICE} = P_{load}$, i.e., the sum of ED power, and ICE power is delivered to the load (the planetary efficiency is ignored for now).

The details of the mode reduction concept, when the HEV is operating, can be described as follows:

- For $v = 0$ ($P_{ED} \geq 0$): the engine-only mode ($P_{ICE} > 0, P_{ED} = 0$) corresponds to zero power flow from the ED which can be achieved by a zero-value of the ED control variable; the motor only mode ($P_{ICE} = 0, P_{ED} > 0$) corresponds to no power flow from the ICE that is also achievable by a zero-value of the engine control variable; in motor assisted mode ($P_{ICE} > 0, P_{ED} > 0$) both ICE power and ED power are strictly positive to the wheels achievable by non-zero control variables of the ED and ICE.
- For $v = 1$ ($P_{ED} < 0$): the regenerative-braking mode ($P_{load} < 0, P_{ED} < 0$) corresponds to a reverse of the ED power flow to charge the battery with ICE power at zero (or nearly so); and the engine-charging-battery mode ($P_{ICE} > 0, P_{ED} < 0$) corresponds to the case when the ED operates as a generator with positive ICE power flow to the ED and possibly to the wheels.

It can be seen that the two modes of operation at the supervisory level coincide with the modes of the ED denoted as $v = 0$ (motoring) and $v = 1$ (generating). The summary of the bi-modal switched system describing the essential dynamics of the power flow at the supervisory level is given next.

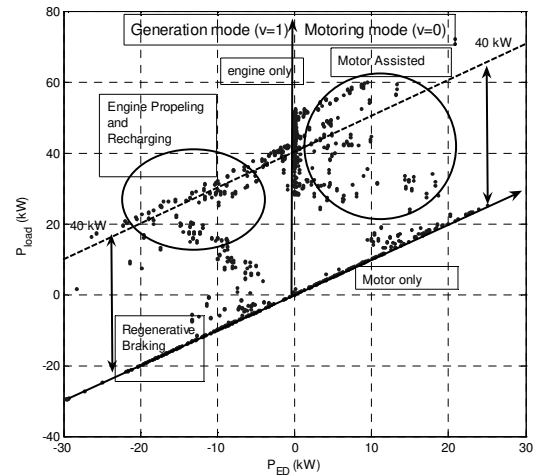


Fig. 2. Power Flow strategy obtained in this study using NMPC tracking EPA highway profile showing the concept of mode reduction from five to two

C. HEV State Model Overview

The summary of the modeling equations, detailed in [31], [32], are summarized in this subsection. The input-output power relationships of subsystems consist of algebraic and dynamical equations. The input-output relationship is considered

algebraic when the its internal power flow dynamics are much faster than others. The essential dynamical state is

$$x(t) \triangleq [P_{ICE}, SOC, V]^T, \quad (1)$$

where P_{ICE} is the ICE power, SOC is the battery state-of-charge, and V is the longitudinal vehicle's velocity. The mode-dependent nonlinear state equation for the PHEV in this study is:

$$\dot{x}(t) = f_{v(t)}(x(t), u_{v(t)}(t)) \quad (2)$$

where $f_v(\cdot)$ denotes the dynamics when motoring, $v = 0$, or when generating, $v = 1$. The modulating controls in modes-0/1 are

$$u_{0/1}(t) = [u_{ICE}(t), u_{FR}(t), u_{EM/GEN}(t)]^T \in \Omega \subset \mathbb{R}^3 \quad (3)$$

where (i) the compact and convex set,

$$\Omega = [0, 1] \times [0, 1] \times [0, 1] \quad (4)$$

(ii) $u_{ICE}(t) \in [0, 1]$ modulates the maximum available ICE power; (iii) $u_{FR}(t)$ modulates the maximum frictional braking; and (iv) $u_{EM/GEN}(t) \in [0, 1]$ modulates the maximum available ED power in the mode-0 and mode-1, respectively.

The motivation for this control structure is four-fold. First, the model is scalable in terms of numbers of power sources (ICE's or ED's) so that the corresponding increase in the number of operating modes leads to only a polynomial increase in complexity for numerical optimization methods [33]. Second, the model has a form compatible with hybrid optimal control theory. Third and more critically, the fact that the controls take values in a convex compact set Ω makes the PMCP amenable to hybrid optimization techniques. Fourth, any optimization algorithm searches for the optimal controls and switching function $v(t)$ in a hypercube as opposed to a (non-convex) state and time-dependent region.

1) *State Equation for the ICE:* The variable P_{ICE} denotes the unidirectional instantaneous ICE power flow, quantified at the flywheel and including losses due to parasitic loads. The ICE dynamical equation is given by equation (5), i.e.,

$$\dot{P}_{ICE} = -\frac{1}{\tau_{ICE}} P_{ICE} + \frac{1}{\tau_{ICE}} P_{ICE}^{\max}(\omega_{ICE}) \cdot \text{eng}(\omega_{ICE}) \cdot u_{ICE}(t) \quad (5)$$

where τ_{ICE} is the nominal engine power delivery delay averaging the effect of the firing delay, smoke limit map, crankshaft speed, fueling shot mode, etc. Further, this also ensures that the command handed down by the supervisory controller can be followed. P_{ICE}^{\max} is an ω_{ICE} -dependent maximum available ICE power; ω_{ICE} is the CVT controller-selected engine speed using the strategy modified slightly from the speed-envelope for a non-hybrid ICE in [34]. Specifically,

$$\omega_{ICE} = (1 - p) \omega_{ICE}^{\min}(V) + p \omega_{ICE}^{\max}(V) \quad (6)$$

where $p \in [0, 1]$ modulates the speed curve according to the ICE power level; $\omega_{ICE}^{\min}(V)$ and $\omega_{ICE}^{\max}(V)$ are the minimum and the maximum allowable speeds at each vehicle's velocity and illustrated in Fig. 3. For better driveability, ICE-CVT's transition from non-engaged to engaged is not allowed when

the vehicle's velocity is too low for jerk reduction. Note that in this study, the capitalized superscript indicates constant whereas lower-case superscripted means parameter dependent.

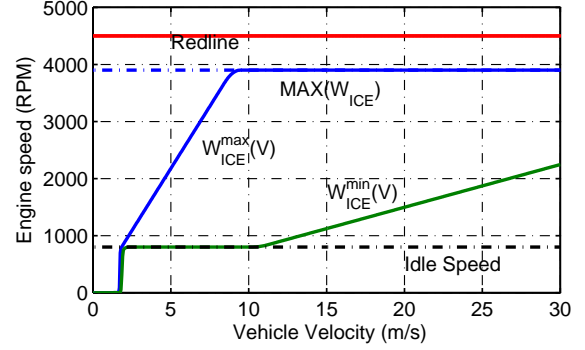


Fig. 3. Maps of minimum and maximum engine speeds for each vehicle's velocity

According to ICE dynamical equation (5), and the constraints on the input, (4), it can be shown that P_{ICE} belongs to the compact and convex set:

$$P_{ICE} \in [P_{ICE}^{MIN}, P_{ICE}^{MAX}] \subset \mathbb{R} \quad (7)$$

The range of ICE power (7) is not an additional state constraint, but rather is a direct result from the aforementioned relationships. This information is useful during the computation of the solution as the numerical search-space is smaller.

2) *State Equation for Battery Operation:* For a relatively new battery, the normalized energy and the SOC are equivalent [35], [36]. The state equation describing the SOC dynamics is derived based on the conservation of power and energy. The parameters are computed to fit the battery data. The partial linearization about the mode-dependent nominal battery operating power, $P_{bat,nom}^v$, describing the SOC is given by:

$$\begin{aligned} \dot{SOC}(t) = & \frac{d_{3,v}}{W_{bat}^{MAX}} \left(P_{bat,nom}^v \right)^2 \\ & - \left[\ln(d_{2,v} + d_{1,v} SOC(t)) + 2d_{3,v} P_{bat,nom}^v \right. \\ & \left. + d_{4,v} \right] \frac{P_{bat}}{W_{bat}^{MAX}} \end{aligned} \quad (8)$$

The validation result of this model against a variety of battery data appear in [37]. In equation (8), W_{bat}^{MAX} is the rated maximum battery energy, P_{bat} is the battery power either drawn by (positive for $v = 0$) or provided by the ED (negative for $v = 1$) and is implicitly controlled by $u_{EM/GEN}$. Specifically,

$$P_{bat} = \begin{cases} P_{ED,in}^0, & v = 0 \\ -P_{ED,out}^1, & v = 1 \end{cases} \quad (9)$$

$d_{k,v}$, $k = 1, \dots, 4$ are the appropriate coefficients. The consideration of the recovery, cycling, and aging effects are beyond the scope of this investigation. This formulation makes equation (8) scalable to a variety of battery storage capacities and types.

3) *State Equation for Vehicle Motion*: The conventional longitudinal vehicle's velocity is described, not in terms of torques, but rather in terms of the acting power flow as:

$$\dot{V} = - \left[\frac{k_w}{m_c} V^2 + k_{v2} \cos(\alpha(t)) \right] \text{sgn}(V) - g \sin(\alpha(t)) + \frac{1000}{m_c(V+\varepsilon_V)} \left[P_{CDD,wh}^v - P_{FR} \right] \quad (10)$$

In equation (10), ε_V is a regularization term; m_c is vehicle mass; $\frac{k_w}{m_c} V^2$ is normalized aerodynamic drag; $k_{v2} \cos(\alpha(t))$ is the rolling resistance; $\alpha(t)$ is the time-varying angle of road inclination; $P_{CDD,wh}^v$ is the power delivered from (≥ 0) and to (< 0) the CDD. Finally,

$$P_{FR} = P_{FR}^{\max}(V) u_{FR}(t) \quad (11)$$

is the frictional braking power. As a result from equation (10), the vehicle's velocity is also in an invariant set,

$$V \in [V^{MIN}, V^{MAX}] \subset R. \quad (12)$$

4) *Mode Dependent ED Modeling Equations*: The derivation of the ED algebraic input-output power flow equations for both modes can be found in [38]. The ED in this study, operated under a maximum torque/amp (MTA) control strategy, can be represented at the supervisory level as

$$P_{ED}^v = \eta_{ED}^v(\omega_{ED}) P_{ED,in}^v \quad (13)$$

Each term in equation (13) is mode dependent. The ED output power is denoted P_{ED}^v , the efficiency $\eta_{ED}^v(\omega_{ED})$ strongly depends on the choice of closed-loop control, a phenomena largely underweighted in the HEV literature; $\omega_{ED} = \beta \cdot V$ is the ED rotor speed; β is a positive constant. The ED input power in modes 0 and 1 is

$$P_{ED,in}^0 = P_{ED,in}^{\max}(\omega_{ED}) \cdot u_{EM}(t) \quad (14)$$

$$P_{ED,in}^1 = P_{ED,in}^{\max}(\omega_{ED}) \cdot u_{GEN}(t) \quad (15)$$

where $P_{ED,in}^{\max}(\omega_{ED})$ is the speed dependent ED maximum input power modulated by the control $u_{EM}(t)$ in mode-0, and $u_{GEN}(t)$ in mode-1.

5) *CVT and mode-dependent CDD Power Flow Equations*: No power response lag between the input and output CVT powers is assumed at the supervisory level, leading to the algebraic equation

$$P_{cvt,out}(t) = \eta_{cvt} P_{cvt,in} \quad (16)$$

where η_{cvt} is the CVT efficiency; $P_{cvt,in}(t) = P_{ICE}$ is the CVT input power; and the output power is delivered to the CDD, i.e., $P_{cvt,out}(t) = P_{CDD,cvt}$.

The CDD's input/output power flows are given by

$$P_{CDD,wh}^0(t) = \eta_{cdd1} P_{CDD,cvt} + \eta_{cdd2} P_{CDD,ED}^0 \quad (17)$$

and

$$P_{CDD,ED}^1(t) = \eta_{cdd2} P_{CDD,cvt} - \eta_{cdd2} P_{CDD,wh}^1 \quad (18)$$

(i) η_{cdd1} , and η_{cdd2} are the appropriate power transfer efficiency among the ED, CVT and wheels; (ii) $P_{CDD,ED}^0 = P_{ED}^0$ is the propulsion power coming directly from the output of the ED in mode-0; in mode-1, $P_{CDD,ED}^1 = P_{ED,in}^1$ is an

output power part of the CDD providing mechanical power to the input of the ED (generator); (iii) in mode-0, $P_{CDD,wh}^0 \geq 0$. However, in mode-1, $P_{CDD,wh}^1(t)$ can be either positive or negative. Note that $P_{CDD,wh}^0$ is represented as P_{load} in the mode reduction concept in Section 2.2.

III. PERFORMANCE INDEX

To incorporate the desired behaviors of the HEV operation, we consider the optimization functional for each mode, as follows:

$$J_v(x_0, u, [t_0, t_f]) = g(t_0, x_0, t_f, x_f) + \int_{t_0}^{t_f} L_v(t, x, u) dt \quad (19)$$

The mode-dependent integrand $L_v(t, x, u)$ depends on the optimization objectives, such as minimizing only fuel consumption as in [39], or a combination of fuel consumption and emissions as in [9], [40], [41]. In this research the PI consists of terms that are consistent with the power flow management framework and have meaningful physical interpretations. The integral quadratic PI that uses the same integrand for both modes of operation, i.e., $L_0(t, x, u) = L_1(t, x, u)$ is adopted in this study. The integrand for both modes is

$$L_v = C_V(V - V^{des}(t))^2 + C_{ICE} \left(\frac{P_{ICE}}{\eta_{ICE}(\cdot)} \right)^2 + C_{FR}(P_{FR})^2 \quad (20)$$

The integrand penalizes the velocity tracking error, $C_V(V - V^{des}(t))^2$, the frictional braking power, $C_{FR}(P_{FR})^2$, and the fuel usage. The fuel usage is approximated by ICE power usage divided by fuel conversion efficiency [42], i.e., $C_{ICE} \left(\frac{P_{ICE}}{\eta_{ICE}(\cdot)} \right)^2 = C_{ICE}(P_{fuel})^2$ where $\eta_{ICE}(P_{ICE}, V)$ is the ICE efficiency that depends on the ICE power-and-speed. Fig. 4 depicts the efficiency map of the ICE superimposed with the iso-efficiency curves.

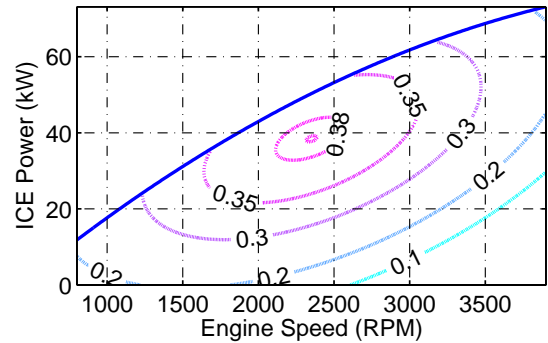


Fig. 4. ICE power-vs-engine speed superimposed with iso-efficiency curves

The penalty on the variation in the boundary conditions, $g(t_0, x_0, t_f, x_f)$, in PI (19) is taken as $C_{bat}(\cdot)(SOC(t_f) - SOC^{NOM})^2$. This choice of the penalty pushes the SOC at t_f toward the nominal level, SOC^{NOM} . It is also desirable to operate the SOC in a predefined range to prolong battery lifetime. It will be shown

in the simulation results that this choice of penalty on the battery SOC can be used to encourage

$$SOC \in [SOC^{MIN}, SOC^{MAX}] \subset \mathbb{R} \quad (21)$$

Note that if the constraints (21) are violated, the penalty term on the SOC must be more stringent. This SOC strategy is intended to enforce a charge-sustaining operation.

A more elaborate PI accounting for drivetrain losses in each mode has the form

$$\begin{aligned} L_v = & C_V^v (V - V^{des}) + C_{ICE}^v (P_{fuel})^2 \\ & + C_{cvt}^v (P_{cvt,loss})^2 + C_{CDD}^v (P_{C,loss}^v)^2 \\ & + C_{ED}^v (P_{ED,loss}^v)^2 + C_{bat}^v (P_{bat,loss}^v)^2 \\ & + C_{FR}^v (P_{FR})^2 \end{aligned} \quad (22)$$

where the additional power loss terms are CVT losses, CDD losses, ED losses, and battery losses, whose identity should be clear from the notation. More details on the generalized PI can be found in [31].

IV. POWER MANAGEMENT CONTROL PROBLEM AND THE EOCP

For the switched optimal control problem (SOCP), the modal switching function $v(t)$ belongs to a discrete set $\{0, 1\}$, $v(t) \in \{0, 1\}$. In contrast, for the EOCP the modal switching function $v(t)$ takes values in the closed interval $[0, 1]$, a continuum of possible values. The enlargement of $v(t) \in \{0, 1\}$ to $v(t) \in [0, 1]$ constitutes an embedding of the SOCP into a larger family of continuously parameterized problems. This embedding converts a non-convex SOCP into a convex EOCP. As per [20] the SOCP can almost always be solved by first solving the EOCP and any solution of the EOCP can be approximated to any degree of precision by some solution of the switched state model (2). Further, in this study, projection techniques are also presented as alternatives for approximating the EOCP solution by an SOCP trajectory.

A. Specification of the embedded optimal control problem

The embedding requires creating a convex combination of the vector fields of the switched state model according to the equation,

$$\begin{aligned} \dot{x}(t) & \triangleq f_E(x(t), u_0(t), u_1(t), v(t)) \\ & = [1 - v(t)] f_0(x(t), u_0(t)) \\ & \quad + v(t) f_1(x(t), u_1(t)) \end{aligned} \quad (23)$$

where $u_i(t) \in \Omega$, $i = 0, 1$. Clearly if $v(t) = 0$, f_E reduces to the 0-mode vector field and similarly for $v(t) = 1$.

The performance index (PI) of the EOCP results from a similar convex embedding of the PIs associated with each mode of operation of the SOCP:

$$\begin{aligned} J_E(x_0, u_0, u_1, v, [t_0, t_f]) & = g(t_0, x_0, t_f, x_f) \\ & \quad + \int_{t_0}^{t_f} L_E(t, x, u_0, u_1, v) dt \\ & = g(t_0, x_0, t_f, x_f) \\ & \quad + \int_{t_0}^{t_f} [(1 - v(t)) L_0(t, x, u_0) \\ & \quad + v(t) L_1(t, x, u_1)] dt \end{aligned} \quad (24)$$

with $L_i(t, x, u_i)$, $i = 0, 1$, denoting the convex-in- u_i integrands of the PI. When $v(t) \in \{0, 1\}$, the minimization of (24) subject to (23) defines the SOCP, while when $v(t) \in [0, 1]$, the minimization of (24) subject to (23) constitutes the EOCP. Formally the EOCP (the structure for solving the PMCP) becomes:

$$\min_{u_0, u_1, v} J_E(x_0, u_0, u_1, v, [t_0, t_f]) \quad (25)$$

with $J_E(\cdot)$ given by (24), subject to

$$\dot{x}(t) = f_E(x(t), u_0(t), u_1(t), v(t)) \quad (26)$$

with f_E given in (23), $v(t) \in [0, 1]$, and $u_0, u_1 \in \Omega$.

B. Relationships between EOCP and SOCP

If the EOCP has a bang-bang type solution (wherein $v(t)$ only takes values in $\{0, 1\}$) then clearly it is also a solution to the original SOCP. Further it can be shown (Corollary 2 in [20]) that the set of trajectories of the switched system (equation (23) with $v(t) \in \{0, 1\}$) is dense in the set of trajectories of the embedded system (equation (23) with $v(t) \in [0, 1]$). Thus when/if the EOCP does not have a bang-bang type solution (wherein $v(t) \in (0, 1)$ for some non-zero measure sets of time) then the EOCP solution can be approximated by a trajectory of the switched system to any desired degree of precision. These relationships between the SOCP and EOCP motivate and justify the effort in determining SOCP solutions by solving the EOCP. Additional relationships between SOCP and EOCP can be found in [20].

C. Approximation to Singularities in EOCP

This subsection describes approximation techniques when the control $v(t)$ obtained via the EOCP is not bang-bang. When, $v(t) \in (0, 1)$, i.e., $v(t)$ takes on fractional values, over an interval $t_1 \leq t \leq t_2$, it would suggest that for the HEV the ED operate simultaneously in both modes for this time interval, an impossibility. In another words, when $v(t) \in (0, 1)$, the SOCP does not have a solution, but epsilon-approximating solutions to the EOCP can be constructed as follows. Given a desired error of approximation, ε , one can construct subintervals $t_1 < T_1 < T_2 \dots < t_2$ such that $|T_{i+1} - T_i| < \delta$, where delta is generated based on ε , vector fields, f_i , and cost integrand, L_i . In the case when the switching interval-constrained by the embedded controller loop time, actuator bandwidth, etc-is larger than δ , one would have to increase the approximating error, ε , and re-construct the intervals. The approximating error will need to be sufficiently large to accommodate the constraint $\delta > T_{\min}$, where T_{\min} is the minimum switching period.

The construction of the switching subintervals in the case of complex vector fields, such as the case for the HEV model, can be alleviated by considering empirical based switching intervals such as described below.

One approach to empirical switching is to average the fractional values of $v(t)$ over $t_1 \leq t \leq t_2$ and the average value, denoted \bar{v} , over $t_1 \leq t \leq t_2$, can be interpreted as a duty cycle, or a pulse width modulation (PWM) control. So there exists a time t' such that for $t_1 \leq t < t'$, the system is

in mode 0 and for $t' \leq t < t_2$ the system is in mode 1 so that the average over the whole interval is $\bar{v} = \frac{t_2 - t'}{t_2 - t_1}$. Thus, a PWM or switched approximation to the embedded $v(t)$ is made.

The previously computed $u_i(t)$ are associated with the embedded solution $v(t)$, not the new approximation. One possibility is to simply use these values for each associated subinterval. A second possibility is to set $v(t)$ equal to its PWM approximation and then find the optimal u_0 and u_1 associated with this choice. Switching can be minimized by beginning the duty cycle for the next interval in the ending mode of the prior interval.

A third possibility is as follows: let T_{\min} be the smallest switching interval of time. For each time unit, $t_1 \leq t \leq t_2 = t_1 + T_{\min}$, one can project the fractional value of $v(t)$ onto the set $\{0, 1\}$ according to the formula:

$$\overline{\|(1 - v(t)) \cdot u_0(t)\|_2} \begin{cases} \geq \overline{\|v(t) \cdot u_1(t)\|_2} \Rightarrow v(t) = 0 \\ < \overline{\|v(t) \cdot u_1(t)\|_2} \Rightarrow v(t) = 1 \end{cases} \quad (27)$$

where over-bars denote averages over the interval $t_1 \leq t \leq t_2 = t_1 + T_{\min}$. As before one can either use the previously calculated values of u_i or resolve the optimization with $v(t)$ fixed at the desired mode. For the simulation studies of this work, equation (27) was used to fix the bang-bang solution for $v(t)$ and then the optimization was resolved for the best pair of $u_i(t)$ given the fixed mode sequence.

D. Embedded PI for PMCP

As mentioned earlier, the integrand and the penalty on the boundary conditions in both modes are the same. The embedded PI for the PMCP is obtained by substituting appropriate terms in the PI (24), i.e.,

$$\begin{aligned} J_E &= C_{bat}(\bullet) (SOC(t_f) - SOC^{NOM})^2 \\ &+ \int_{t_o}^{t_f} \left(C_V (V - V^{des}(t))^2 \right. \\ &+ C_{ICE} \left(\frac{P_{ICE}}{\eta_{ICE}(\bullet)} \right)^2 \\ &\left. + C_{FR} (P_{FR}^{MAX}(\bullet) u_{FR}(t))^2 \right) dt \end{aligned} \quad (28)$$

where the physical meaning of each term is given in Section 3.

V. SUMMARY ON THEORETICAL FOUNDATIONS

When the discrete input $v \in \{0, 1\}$ presents, it renders, in general, the SOCP non-convex. For a variety of assumptions on system vector fields f_v , an SOCP performance index, and mode-switching penalties and constraints, several approaches have been employed in the literature for characterizing and computing SOCP solutions, consisting of: searches over or assumptions on mode sequences and switching instants, after which one computes the continuous control values and the cost to compare the different scenarios. These approaches do not allow the switching function to be chosen in concert with the continuous time control as is the case with the embedded approach.

Discussing neither sufficient conditions for optimality nor account for the singular solution scenarios, Riedinger et al.

(1999) applies directly the Maximum Principle to the SOCP. For a larger class of systems, and with a cost that depends on the mode sequence, Sussmann (1999) derives necessary conditions for optimality via a generalized Maximum Principle. Other approaches include pre-assigned switching sequence method (for a limited class of problems) in [43], and a hybrid Bellman inequality approach in [44]. Mixed integer programming (MIP) approaches have also been employed to find optimal solutions [19]. Solving the problem using MIP methods, however, is non-deterministic polynomial-time hard (NP-hard); indeed the scalability of this technique is problematic [45].

The nonconvexity of the problem and the inapplicability of the mentioned existing techniques—too general and impractical, or very specific results, or insufficient characterization of solutions—to the SOCP has led to the development of the parameterized family of problems, the EOCP, set forth in the previous section.

A. EOCP: Sufficient Existence Conditions

This section summarizes the main sufficient conditions for EOCP solutions. Sufficient conditions for optimality are [Theorem 9, in [20]]:

- (i) the admissible pair set (control, trajectory) is nonempty;
- (ii) the points $(t, x(t))$ are included in a compact set for all $t \in [t_0, t_f]$;
- (iii) the terminal set is compact;
- (iv) the input constraint set is compact and convex;
- (v) the vector fields f_0 and f_1 are linear in their (control) inputs u_0 , and u_1 , respectively i.e.,
 - (S1) $f_0(t, x, u_0) = A_0(t, x) + B_0(t, x)u_0$
 - (S2) $f_1(t, x, u_1) = A_1(t, x) + B_1(t, x)u_1$
- (vi) for each $(t, x(t))$, the integrands of the penalty functions, $L_0(t, x, u_0)$ and $L_1(t, x, u_1)$, are convex functions of u_0 , and u_1 , respectively.

Based on the assumptions made on the input constraint set and on the vector fields f_0 and f_1 , one can conclude that conditions (i), (ii), and (iv) are met. Further, a sufficiently large compact set can be substituted for the terminal set, meeting condition (iii). Condition (v) is also met as it can be observed based on the modeling equations from Sections 2. Specifically, the power terms that depend on the continuous control inputs, are factored into the product of a control input and a term that depends on the state, $x(t)$. Utilizing the form of these power terms, and the forms of $L_0(t, x, u_0)$ and $L_1(t, x, u_1)$ one concludes that condition (vi) is also met. Hence the EOCP has a solution.

The above sufficient conditions only guarantee the existence of the EOCP's solutions, but do not provide a solution methodology. In conjunction with the SOCP-EOCP relationships mentioned above, the necessary conditions obtained by direct application of the Maximum Principle [38] provide a method for obtaining at least suboptimal solutions of the SOCP. By using this approach, the optimization problem is transformed into a two-point boundary value problem on the state and adjoint equations. The single shooting method is applied to compute the numerical solution in [25], and the solution is

very sensitive with respect to the co-state initial condition. The multiple shooting method can be applied to reduce the sensitivity issue. This paper takes an alternate approach for computing numerical solutions to the EOCP, i.e., via the direct collocation method, described in the next section.

VI. NUMERICAL TECHNIQUE AND NMPC

This section briefly describes the direct collocation method and the nonlinear model predictive control (NMPC) strategy. Both are used in conjunction to formulate the PMCP as a nonlinear programming problem (NLP).

A. Discretization via Direct Collocation

Given the PI (28) and the state equation and constraints of equations (23), one discretizes these equations using the direct collocation method. The discretization of the PI uses a variation of the trapezoidal rule and constraint equations use the mid-point rule, respectively. These discretized equations convert the EOCP into a finite dimensional NLP where states and inputs are treated as unknown variables. The direct collocation technique consists of several steps that have two main stages: (i) time discretization, and state and input function approximations by a finite number of polynomial basis functions; (ii) approximation of the continuous state dynamics and cost index integrand by discrete-state and discrete-input-dependent counterparts.

Without going through a lengthy derivation, the continuous time interval $[t_0, t_f]$ is discretized into a sequence of points $t_0 < t_1 < t_2 < \dots < t_{N-1} < t_N = t_f$ where, for simplicity, we take $t_j - t_{j-1} = h$, for $j = 1, \dots, N$. A "hat" notation is also used to distinguish the numerically estimated state and control values from their actual counterparts that are "hatless", e.g., $\hat{x}_j = \hat{x}(t_j)$, $\hat{u}_{0,j} = \hat{u}_0(t_j)$, $\hat{u}_{1,j} = \hat{u}_1(t_j)$ and $\hat{v}_j = \hat{v}(t_j)$. The collocation method used here assumes triangular basis functions for the state and piecewise constant basis functions (derivatives of triangular functions) for the controls. Specifically, the estimated state is given by

$$\hat{x}(t) = \sum_{j=0}^N \hat{x}_j \varphi_j(t) \quad (29)$$

where the \hat{x}_j 's are to be determined and the triangular basis functions are given by

$$\varphi_j(t) = \begin{cases} \frac{t-t_{j-1}}{h}, & t_{j-1} < t \leq t_j \\ \frac{t_{j+1}-t}{h}, & t_j < t \leq t_{j+1} \\ 0, & \text{elsewhere} \end{cases} \quad (30)$$

We note two points: the method is not restricted to using triangular basis functions and each of the $\varphi_j(t)$'s is a time shift of the previous one.

As summarized in [24], the theoretical approach for computing the controls is to extend the state space with new state variables, $x_{ext} \in R^{m+1}$, whose derivative are the desired controls, $u(t) \in R^m$ and $v(t) \in [0, 1] \subset R$, to be computed. However, our choice of triangular basis functions for the states renders the control inputs piecewise constant and we simply

solve directly for these (constant) control values. Specifically, the estimates of the control inputs are given by

$$\begin{bmatrix} \hat{u}(t) \\ \hat{v}(t) \end{bmatrix} = \sum_{j=1}^N \begin{bmatrix} \hat{u}_j \\ \hat{v}_j \end{bmatrix} \psi_j(t) \quad (31)$$

where the piecewise constant basis functions are given by

$$\psi_j(t) = \begin{cases} 1 & t_{j-1} < t \leq t_j \\ 0 & \text{elsewhere} \end{cases} \quad (32)$$

The essence of the midpoint rule in the collocation method is to enforce the constraints at the midpoints of each interval $[t_{j-1}, t_j]$ for $j = 1, \dots, N$. There results the discretized embedded state dynamics

$$\begin{aligned} \hat{x}_j &= \hat{x}_{j-1} + h \cdot (1 - \hat{v}_j) \cdot f_0 \left(\frac{\hat{x}_{j-1} + \hat{x}_j}{2}, \hat{u}_{0j} \right) \\ &+ h \cdot \hat{v}_j \cdot f_1 \left(\frac{\hat{x}_{j-1} + \hat{x}_j}{2}, \hat{u}_{1j} \right) \end{aligned} \quad (33)$$

for $j = 1, \dots, N$, with $f_0(\cdot)$ and $f_1(\cdot)$ the discretized state dynamics in modes -0 and -1, respectively. Thus, the solution to the EOCP is given by the following NLP: Minimize

$$\begin{aligned} \hat{J}_E &= C_{bat}(\cdot) \left(\hat{SOC}_N - SOC^{NOM} \right)^2 \\ &+ \sum_{j=1}^N \frac{1}{2} h \{ L_E(t_j, \hat{x}_j, \hat{u}_{0j}, \hat{u}_{1j}, \hat{v}_j, \hat{p}_j) \\ &+ L_E(t_{j-1}, \hat{x}_{j-1}, \hat{u}_{0j}, \hat{u}_{1j}, \hat{v}_j, \hat{p}_j) \} \end{aligned} \quad (34)$$

over the controls $(\hat{u}_j, \hat{v}_j) \in \Omega \times [0, 1]$, subject to equation (33) and all other equality/power flow constraints represented as $g(\hat{x}_{j-1}, \hat{x}_j, \hat{u}_j, \hat{v}_j, \hat{p}_j) = 0$. Here $L_E(\cdot)$ is the integrand of equation properly discretized and \hat{p}_j represents the various power flows in the model.

B. Nonlinear Model Predictive Control

The NMPC solution strategy in this study uses a moving four-second predictive-window with the control applied over one-second sub-interval. In particular the NLP for $t = t_j$ is solved over $[t_j, t_{j+1}, t_{j+2}, t_{j+3}, t_{j+4}]$ instead of the entire driving cycle. The resulting control at each iteration is applied only over $[t_j, t_{j+1}]$ to the system model. Using the constant controls computed by NMPC algorithm, the system model is then simulated over $[t_j, t_{j+1}]$ to obtain an updated state at t_{j+1} . This updated state represents what would be measured in a real-world implementation of the NMPC control [28], [46].

We let $t_{f,j}$ denote the final time of each NMPC iteration, and hence is the final time in the PI (28). Further for the NMPC strategy the coefficient penalizing the deviation from nominal SOC, $C_{bat}(t_{f,j})$ is linearly interpolated according to the equation

$$C_{bat}(t_{f,j}) = (t_{f,j}/t_f) C_{bat}^{nom} \quad (35)$$

Otherwise, the NMPC control will try to maintain the SOC at SOC^{NOM} over each iteration unduly restricting the use of battery power.

Difficulties arise for real world implementation since this strategy presumes knowledge of t_f . Nevertheless, it can be

entered by drivers, or becomes an adaptive function of the recent history of the vehicle's power consumption. The estimation problem of t_f is beyond the scope of this paper.

In the beginning of each NMPC window, we assume the knowledge of the current road grade (e.g., through an accelerometer or future GPS). The control algorithms assume that over each partition of the NMPC window, the road grade is constant at the value at the beginning of the NMPC window. Although the road grade may change over the NMPC window, since the control is only applied over the first partition, after which a new measurement is taken, potential error is believed negligible.

VII. SIMULATION RESULTS

The NLP of the PMCP is applicable to various numerical solvers such as AIMMS, TOMLAB, etc. In this study, a sequential quadratic programming (SQP) based NLP solver, *fmincon*, is adopted. This section details simulation results for PHEV tracking different driving profiles. The first set of simulations compare the overall hybrid optimal control and the NMPC tracking the sawtooth driving profile with road grades. The next simulation details the PHEV tracking the standard 765 s EPA Highway driving profile to which is added a sinusoidal road grade to better exercise the controller performance. The second simulation looks at the 600 s US06 FTP supplemental driving schedule. The numerical solutions to various driving profiles are shown below.

A. Optimal and NMPC Tracking of Sawtooth Velocity Profile with Road Grades: Cases 1 and 2

The performances of the overall hybrid optimal control and the NMPC strategies are compared using the sawtooth driving profile suggested in [32]. The sawtooth profile demands higher rates of acceleration/deceleration than typical driving cycles. To further test the limits of performance of the vehicle powertrain, positive sinusoidal road grades are superimposed in this paper.

The coefficients of the PI (28) are $C_V = 10$, $C_{ICE} = 10^{-3}$, $C_{FR} = 10^{-4}$, and $C_{bat}(\cdot) = C_{bat}^{mom} = 10^5$. This study compares the performances of two hybrid optimal control strategies. Case 1 uses a control that minimizes the PI of (28) with the above coefficients over the entire driving cycle and is thus optimal over the driving cycle. Case 2 constructs an NMPC version that can be compared to the optimal solution. Figure 5 shows that initially the vehicle in both cases fail to provide perfect tracking. Initial tracking error is due to the insufficient available propelling power from the ICE and ED both of which already operate at their maximum levels, as shown in Fig. 6 for case 1. As per Fig. 6(a), the ICE is off at startup (propelling from ED alone) due to the closed-loop local control constraint, until a minimum operating speed of 800 RPM is reached. Further, the tracking error during the first 14 s for the NMPC version is larger due to the fact that the NMPC decides to turn the ICE on slightly later. The rest of the driving profiles except the peak at 30 s can be tracked relatively well in both cases.

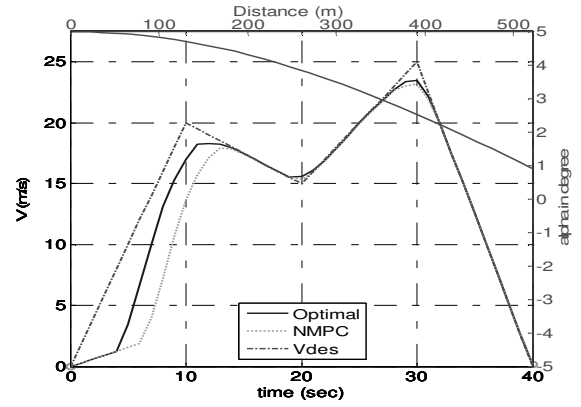
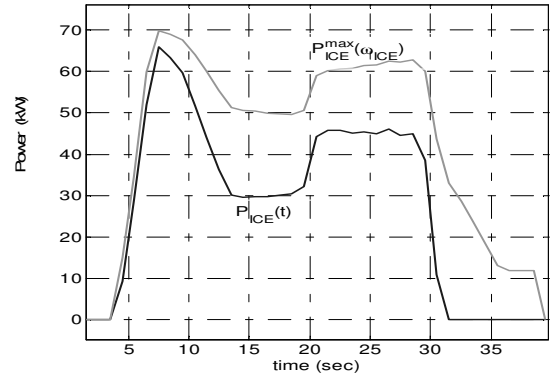
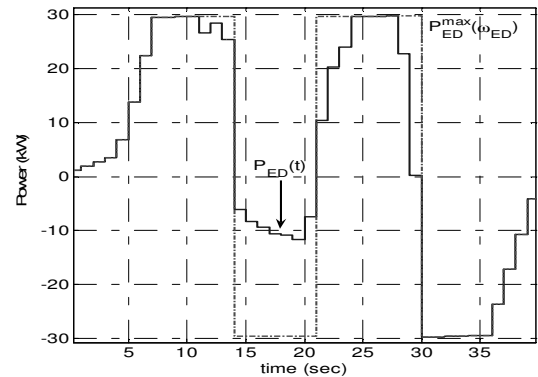


Fig. 5. Velocity tracking performance for overall optimal hybrid control and NMPC tracking sawtooth profile with road grades



(a) ICE power



(b) ED power

Fig. 6. Output power for tracking sawtooth profile with road grades in case 1

After 30 s, when the desired velocity is decreasing and the road grades are positive but small; the ICE is turned off (Fig. 6(a)) and the ED provides negative power to charge the battery in both cases as shown in Fig. 6(b). Between 14 and 21 s the ICE in case 1 provides power both to charge the battery and to the wheels, while in case 2, the ICE only provides propelling power. The ICE profiles in this specific region for the NMPC

are lower and circled in Fig. 7(a). This contributes to slightly better fuel economy for the NMPC version of 14.7 MPG vs. 14.2 MPG for case 1.

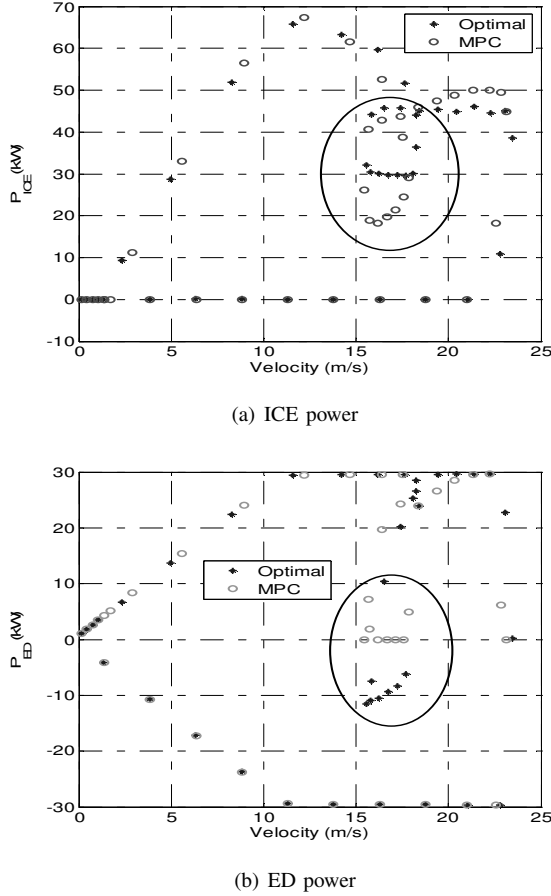


Fig. 7. Output profiles vs vehicle's velocity for overall optimal hybrid control and NMPC tracking sawtooth with road grades showing ICE power and ED power

Simultaneously, the ED in case 1 operates as a generator (mode-1) more often, specifically between 14 and 21 s, as depicted in Fig. 6(b) and Fig. 7(b). The NMPC hands down a non-generating decision in this time interval because of a relatively lower penalty (coefficient) on the deviation from nominal SOC according to (35).

Figure 8 depicts the battery SOC profiles. Case 1 shows consistency with the mode of operation and returns to the vicinity of the 60% nominal level at the end of the cycle.

In case 2, SOC deviation is only mildly penalized allowing lower levels than in case 1 during the first half cycle. In the second half of the driving cycle, with an increasing penalty on the deviation from nominal SOC, the NMPC tries to recharge the battery and returns SOC to the level slightly lower than in case 1.

During the last 10 s, the ED operates as a generator in both cases as expected to provide regenerative braking power. Further, the demanded power is more (negative) than the maximum level that the ED can deliver in both cases as shown in Fig. 6(b). To achieve the desired velocity tracking, the extra kinetic energy is expended in frictional braking as shown in

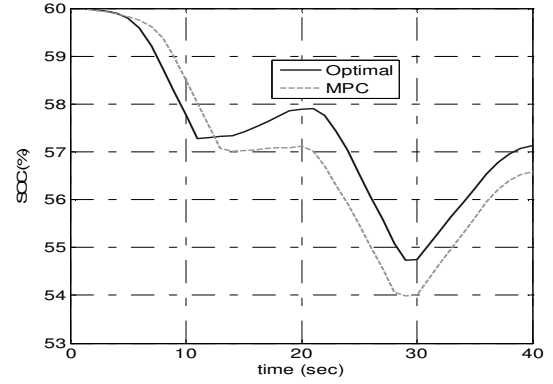


Fig. 8. Battery SOC for overall optimal hybrid control and NMPC tracking sawtooth with road grades

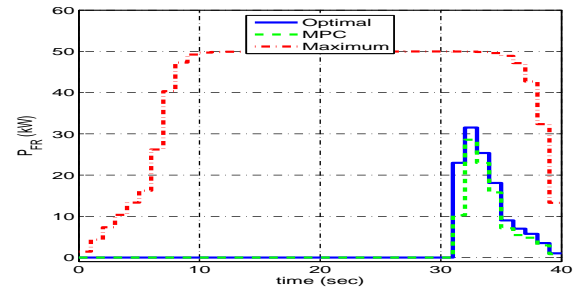


Fig. 9. Frictional-braking power for overall optimal hybrid control and NMPC tracking sawtooth with road grades

Fig. 9. Indeed, frictional braking is only used during the last 10 s of the driving profile as one would expect.

B. NMPC Tracking of EPA Highway Driving Cycle with Road Grade: Case 3

In this case study, the vehicle is to follow the EPA highway driving profile for 765 seconds on a nonzero road grades as shown in Fig. 10. Also shown (solid sinusoidal) in Fig. 10, is the road grades, which has a positive angle (uphill) over the first 382.5 s, and then has a negative angle (downhill) over the final 382.5 s

The coefficients of the PI (28) are the same as those used in the sawtooth driving profiles with a sliding penalty on the deviation of the SOC from nominal as $t \rightarrow t_f = 765$ s Fig. 10 shows that the NMPC strategy provides nearly perfect tracking for this case.

Since there is very little penalty on battery usage initially (see (35)) and a relatively significant penalty on fuel consumption, mode 0 is active for 135 s (Fig. 11(a)) at which the desired velocity starts to decrease.

Initially, the ED supplies roughly 20 kW of propelling power, and eventually decays to near zero at 135 s. In contrast, the ICE is initially off, and gradually ramps to supply propulsion demand reach 40 kW at roughly 135 s (Fig. 13). In other words, the NMPC strategy decides to drain the power from the ED-battery pack to as low as 45% during this time period as shown in Fig. 11(b).

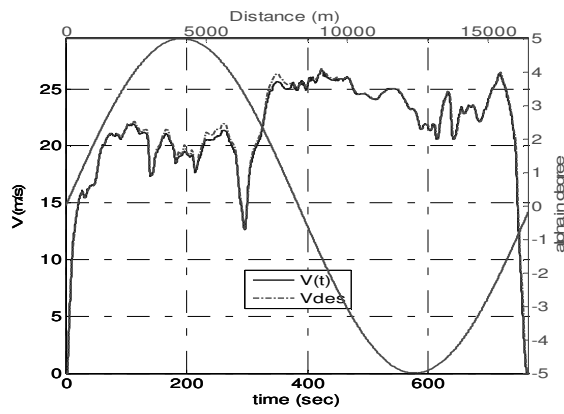


Fig. 10. Velocity tracking performances for case 3 on a road grades whose angle in degrees is indicated by the sinusoidal curve with values in degrees on the right vertical axis

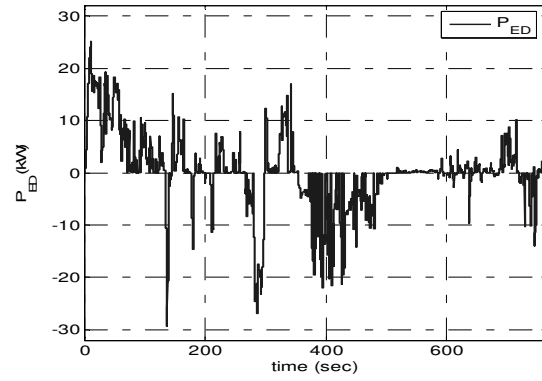
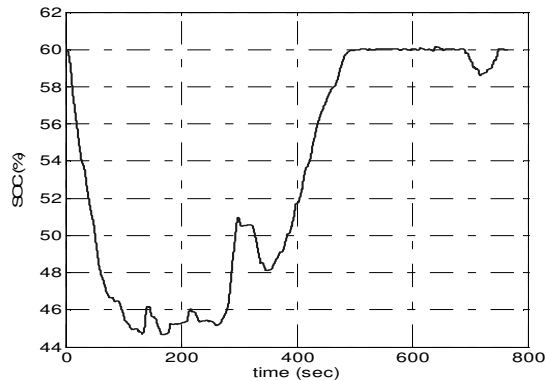
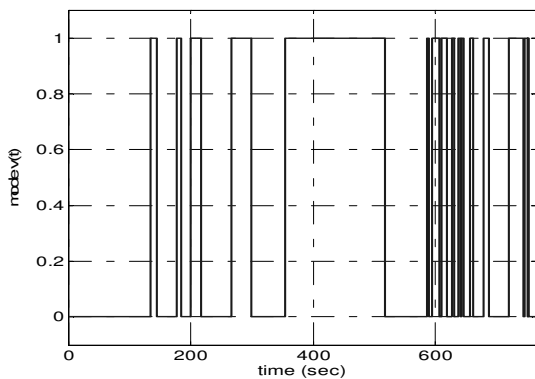


Fig. 12. ED output power profiles for PHEV tracking EPA highway using NMPC strategy



(a) Mode of operation



(b) Battery SOC

Fig. 11. NMPC strategy for tracking EPA highway profile showing Mode of operation and Battery SOC Profiles

After 60 seconds, the ICE power contribution continues to ramp and then remains relatively constant at about 45 kW until 400 seconds as per Fig. 13. Over this period, fuel efficiency is relatively high according to the ICE efficiency map in Fig. 4.

Around 260 sec, the road profile becomes less demanding and the vehicle operates in the generating mode more often.

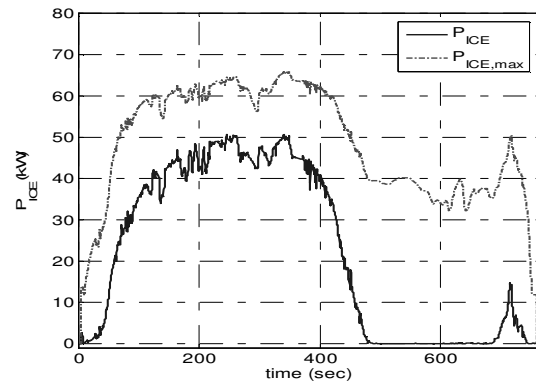


Fig. 13. ICE power usages for PHEV tracking EPA highway using NMPC strategy

Further, after 382.5 sec, the road grades are negative, which leads to regenerative braking. Figure 12 shows that the ED operates more frequently in the generating mode for recharging the battery back to its nominal value of 0.6. Further, there is little need for propelling power to maintain perfect tracking, hence the ICE is off most of the time in the second half of the driving cycle.

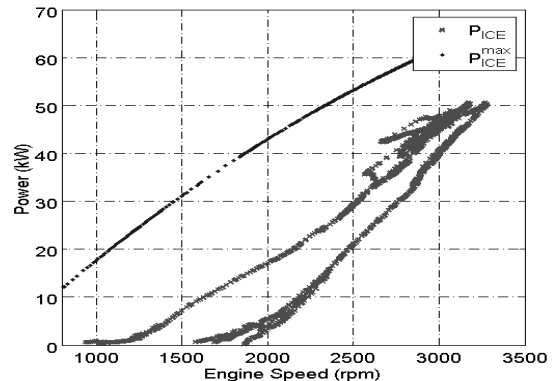


Fig. 14. Trajectories of ICE power vs. engine speed for PHEV tracking EPA highway using NMPC strategy showing acceleration/deceleration hysteresis

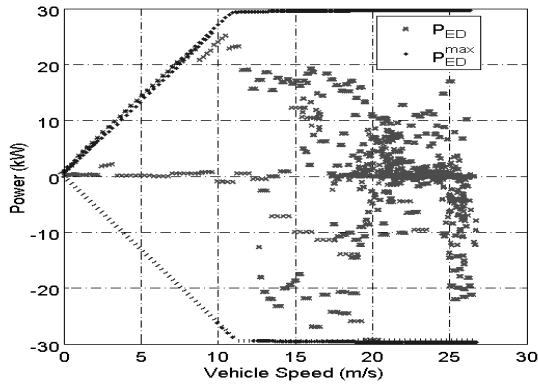


Fig. 15. Trajectories of ED power vs. vehicle for PHEV tracking EPA highway profile using NMPC

The map of the ICE power over the engine speeds' range shows denser data in the fuel efficient region. Hysteresis appears as the result of the dynamics (lag) in the engine power during the acceleration and deceleration as shown in Fig. 14. Figure 15 shows the operation of the ED over the range of vehicle speeds.

In the presence of the sinusoidal road grade over the cycle, the fuel economy is 27.5 mpg, lower than the 32 mpg (similar to current hybrid SUVs on the market) when the road is flat due to (i) frictional braking losses during the negative road grades to maintain velocity tracking and (ii) inefficiencies in energy recovery from regenerative braking. The simulation result in the case of vehicle tracking the EPA highway velocity profile on a flat road is not included in this paper due to space limitations, but it can be found in [31].

One concludes that the NMPC strategy performs very well while sustaining the constraint on the final SOC. Further, the resulting power distributions in this case study is used to justify the concept of five-to-two mode reduction as shown in Fig. 2. The 40 kW line is drawn in the figure to indicate a rough ICE power level that is fuel efficient for a medium engine-speed range.

C. MPC Tracking of the US06 supplemental FTP Driving Profile: Case 4

In this case study, we again use NMPC to track the 600 second US06 supplemental FTP driving schedule, which demands higher accelerations and more aggressive velocity variation/limits than the standard EPA city and highway schedules as shown in Fig. 16. The coefficients of the PI are the same as those in the previous cases. Figure 16 again shows that the NMPC almost perfectly tracks the desired velocity profile.

The aggressive nature of the velocity profile forces the ED to operate close to maximum power levels in both modes (Fig. 17(a)) while the power usage of the ICE mimics (Fig. 17(b)) the shape of the velocity profile.

To meet the transient acceleration demands, NMPC puts the ED in the motoring mode during acceleration and in the generating mode during deceleration. During the non-transient power demand, the middle of the driving cycle, the ED is often

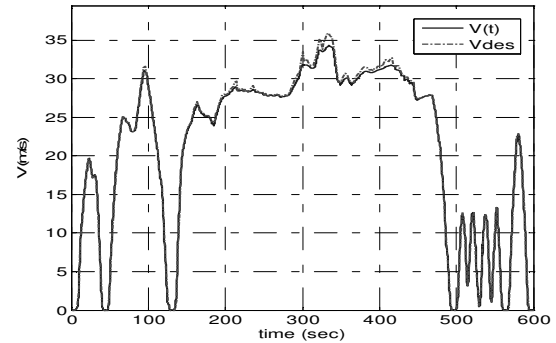
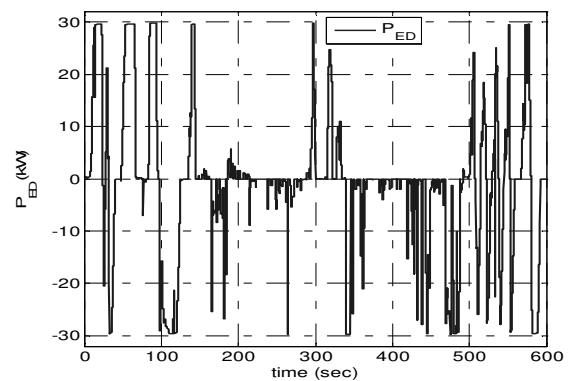
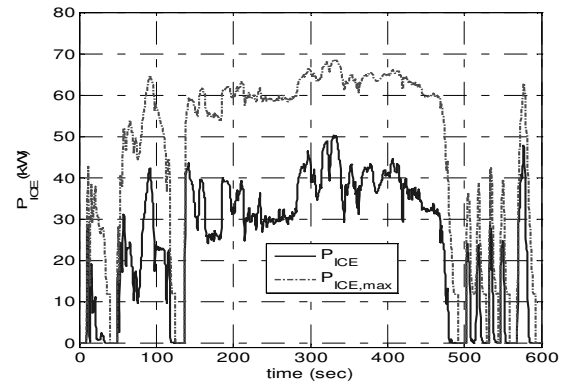


Fig. 16. US06 supplemental FTP driving profile and vehicle tracking performance



(a) ED output power



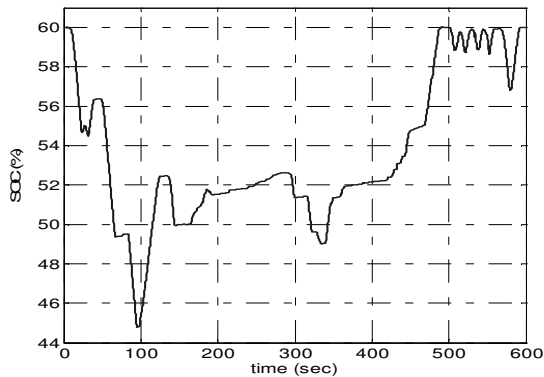
(b) ICE output power

Fig. 17. Plots of ED output power and ICE output power profiles in case 4

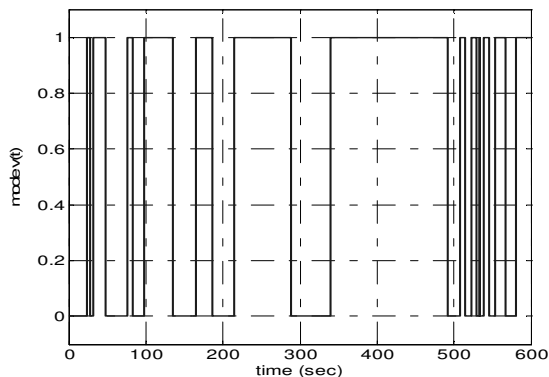
off or provides relatively low power and the ICE provides most of the power as it can operate around its more fuel efficient level. Overall, estimated fuel efficiency averages at 23 mpg, a lower value than the EPA highway profile of 32 due to the more aggressive power demands of this case study.

During the first 100 sec of the driving schedule, the HEV operates primarily in the motoring mode draining the battery to an SOC of about 45 percent as shown in Fig. 18(a). The aggressive acceleration driving profile in concert with the

relatively low penalty on the SOC deviation from the nominal level contributes to the NMPC selection of this strategy. Afterward, as the penalty on the SOC deviation increases linearly toward the final time of 600 sec, the SOC rises toward the nominal level of 0.6 with more frequent time in mode 1.



(a) Battery SOC



(b) Mode of operation

Fig. 18. Case 4: Battery SOC and Mode of operation profiles

Mode switching in both cases, using the strategy outlined in section 4.3, is reasonable, and consistent with the velocity variations in the driving profile as shown in Fig. 18(b).

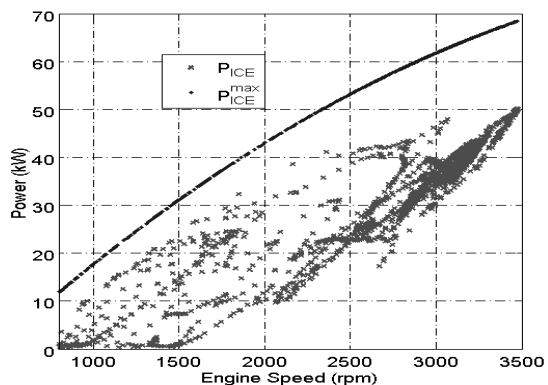


Fig. 19. Trajectories of ICE power vs. engine speed for PHEV tracking US06 FTP profile using NMPC strategy

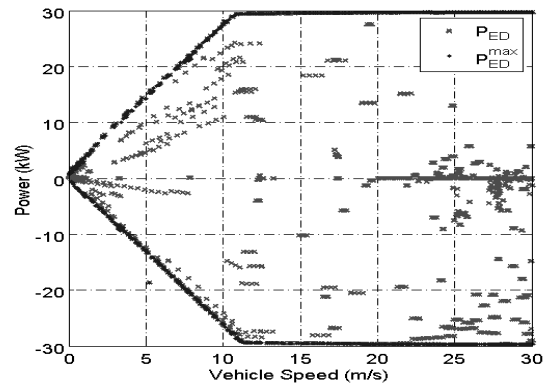


Fig. 20. Trajectories of ED power vs. vehicle for PHEV tracking US06 FTP profile using NMPC strategy

Similar to case 3, the nature of the modified speed envelope strategy for the CVT dictates higher engine speed for higher ICE power as depicted in Fig. 19. Dense engine data is located around 40 kW. In contrast to case 3, wider spread in the trajectories of the ICE on the power-vs-speed map can be observed in this case. Frequent operations on the ED maximum power-vs-speed envelope (in both motoring and generating) are also observed in this case, as depicted in Fig. 20. These characteristics in the ICE and the ED power profiles reflect greater variety of demands in the US06 FTP profile.

D. CONCLUSIONS

An application of the hybrid optimal control for solving the power management control problem (PMCP) in a parallel electric hybrid vehicle (PHEV) has been illustrated in this paper. The advantages outlined in [20] motivate solving for the optimal/suboptimal power flow as the solution to the embedded version of the problem, i.e., the EOCP. The solution of the EOCP can be obtained via a number of numerical techniques.

In this study, the numerical solution is obtained by converting the original infinite dimensional problem into a finite dimensional nonlinear programming problem (NLP) using the direct collocation technique. Then, the resulting NLP is solved via a sequential quadratic programming algorithm. Requiring a short predictive window, the NMPC strategy is applied to solve the PMCP for the sawtooth, EPA highway, and US06 supplemental FTP driving profiles. The simulations show that the NMPC can track the driving profiles quite well unless there is insufficient available power to achieve the tracking as illustrated in case of the sawtooth profile with positive road grades. In practice, vehicle control strategies are often PID and maps/look-up tables based. The resulting NMPC profiles can help providing additional information on how to improve the existing look-up tables or tuning the gain-scheduling maps in the PID based controllers.

REFERENCES

- [1] O. Erdinc, B. Vural, and M. Uzunoglu, "A wavelet-fuzzy logic based energy management strategy for a fuel cell/battery/ultra-capacitor hybrid

- vehicular power system," *Journal of Power Sources*, vol. In Press, Corrected Proof, 2009.
- [2] A. Pesaran, J. Gonder, and M. Keyser, "Ultracapacitor applications and evaluation for hybrid electric vehicles," in *Advanced Capacitors World Summit 2009*, (La Jolla, California), 2009.
 - [3] F. Barbir, H. Gorgun, and X. Wang, "Relationship between pressure drop and cell resistance as a diagnostic tool for pem fuel cells," *Journal of Power Sources*, vol. 141, no. 1, pp. 96–101, 2005.
 - [4] J. B. Cao and B. G. Cao, "Neural network sliding mode control based on on-line identification for electric vehicle with ultracapacitor-battery hybrid power," *International Journal of Control, Automation and Systems*, vol. 7, no. 3, pp. 409–418, 2009.
 - [5] D. Feroldi, M. Serra, and J. Riera, "Energy management strategies based on efficiency map for fuel cell hybrid vehicles," *Journal of Power Sources*, vol. 190, no. 2, pp. 387–401, 2009.
 - [6] Q. Shen, M. Hou, X. Yan, D. Liang, Z. Zang, L. Hao, Z. Shao, Z. Hou, P. Ming, and B. Yi, "The voltage characteristics of proton exchange membrane fuel cell (pemfc) under steady and transient states," *Journal of Power Sources*, vol. 179, no. 1, pp. 292–296, 2008.
 - [7] T. E. Springer, T. A. Zawodzinski, and S. Gottesfeld, "Polymer electrolyte fuel cell model," *Journal of the Electrochemical Society*, vol. 138, no. 8, pp. 2334–2342, 1991.
 - [8] G. Q. Ao, J. A. Qiang, H. Zhong, L. Yang, and B. Zhuo, "Exploring the fuel economy potential of isg hybrid electric vehicles through dynamic programming," *International Journal of Automotive Technology*, vol. 8, pp. 781–790, Dec 2007.
 - [9] C.-C. Lin, P. Huei, J. W. Grizzle, and K. Jun-Mo, "Power management strategy for a parallel hybrid electric truck," *IEEE Trans. Control Syst. Technol.*, vol. 11, no. 6, pp. 839–49, 2003.
 - [10] P. Pisu and G. Rizzoni, "A comparative study of supervisory control strategies for hybrid electric vehicles," *IEEE Transactions on Control Systems Technology*, vol. 15, no. 3, pp. 506–518, 2007.
 - [11] G. Rizzoni, L. Guzzella, and B. M. Baumann, "Unified modeling of hybrid electric vehicle drivetrains," *IEEE/ASME Transactions on Mechatronics*, vol. 4, no. 3, pp. 246–257, 1999.
 - [12] J. Scordia, M. Desbois-Renaudin, R. Trigui, B. Jeanneret, F. Badin, and C. Plasse, "Global optimisation of energy management laws in hybrid vehicles using dynamic programming," *International Journal of Vehicle Design*, vol. 39, no. 4, pp. 349–367, 2005.
 - [13] J. M. Lee and J. H. Lee, "Value function-based approach to the scheduling of multiple controllers," *Journal of Process Control*, vol. 18, no. 6, pp. 533–542, 2008.
 - [14] W. B. Powell, "What you should know about approximate dynamic programming," *Naval Research Logistics*, vol. 56, no. 3, pp. 239–249, 2009.
 - [15] N. Kim, S. Cha, and H. Peng, "Optimal control of hybrid electric vehicles based on pontryagin's minimum principle," *IEEE Transactions on Control Systems Technology*, 2010. cited By (since 1996) 0; Article in Press.
 - [16] N. J. Schouten, M. A. Salman, and N. A. Kheir, "Energy management strategies for parallel hybrid vehicles using fuzzy logic," *Control Engineering Practice*, vol. 11, no. 2, pp. 171–177, 2003.
 - [17] W. Xiong, Y. Zhang, and C. Yin, "Optimal energy management for a series-parallel hybrid electric bus," *Energy Conversion and Management*, vol. 50, no. 7, pp. 1730–1738, 2009.
 - [18] S. Kermani, S. Delprat, R. Trigui, and T. M. Guerra, "Predictive energy management of hybrid vehicle," in *IEEE Vehicle Power and Propulsion Conference*, 2008 IEEE Vehicle Power and Propulsion Conference, VPPC 2008, (Harbin), 2008.
 - [19] A. Bemporad and M. Morari, "Control of systems integrating logic, dynamics, and constraints," *Automatica*, vol. 35, no. 3, pp. 407–27, 1999.
 - [20] S. C. Benghea and R. A. DeCarlo, "Optimal control of switching systems," *Automatica*, vol. 41, no. 1, pp. 11–27, 2005.
 - [21] C. P. Neuman and A. Sen, "A suboptimal control algorithm for constrained problems using cubic splines," *Automatica*, vol. 9, pp. 601–13, 1973.
 - [22] A. Schfer, P. Khl, M. Diehl, J. Schlder, and H. G. Bock, "Fast reduced multiple shooting methods for nonlinear model predictive control," *Chemical Engineering and Processing: Process Intensification*, vol. 46, no. 11, pp. 1200–1214, 2007.
 - [23] O. Von Stryk, "Numerical solution of optimal control problems by direct collocation. in optimal control/calculus of variations, optimal control theory, and numerical methods," *International Series of Numerical Mathematics*, vol. 111, pp. 129–143, 1993.
 - [24] M. Žefran, *Continuous Methods for Motion Planning*. PhD thesis, University of Pennsylvania, Philadelphia, 1996.
 - [25] K. Uthaichana, S. Benghea, and R. DeCarlo, "Suboptimal supervisory level power flow control of a hybrid electric vehicle," in *Proc. of IFAC World Congress*, (Prague), July 2005.
 - [26] M. Diehl, H. G. Bock, H. Diedam, and P. B. Wieber, "Fast direct multiple shooting algorithms for optimal robot control," in *Fast Motions in Biomechanics and Robotics* (M. Diehl and K. Mombaur, eds.), vol. 340 of *Lecture Notes in Control and Information Sciences*, pp. 65–93, Springer, 2006.
 - [27] D. DeHaan and M. Guay, "A new real-time perspective on non-linear model predictive control," *Journal of Process Control*, vol. 16, no. 6, pp. 615–624, 2006.
 - [28] F. Martinsen, L. T. Biegler, and B. A. Foss, "A new optimization algorithm with application to nonlinear mpc," *Journal of Process Control*, vol. 14, no. 8, pp. 853–865, 2004.
 - [29] C. A. Floudas, *Nonlinear and Mixed-Integer Optimization: Fundamentals and Applications*. New York: Oxford University Press, 1995.
 - [30] G. L. Nemhauser and L. A. Wolsey, *Integer and Combinatorial Optimization*. Discrete Mathematics and Optimization, New York: Wiley-Interscience, 1988.
 - [31] K. Uthaichana, *Modeling and control of a parallel hybrid electric vehicle*. PhD thesis, Purdue, West Lafayette, December 2006 2006.
 - [32] K. Uthaichana, S. Benghea, R. DeCarlo, S. Pekarek, and M. Žefran, "Hybrid model predictive control tracking of a sawtooth driving profile for an hev," in *Proceedings of the American Control Conference*, 2008 American Control Conference, ACC, (Seattle, WA), pp. 967–974, 2008.
 - [33] P. Gill, W. Murray, and M. Wright, *Practical Optimization*. Academic Press, 1981.
 - [34] R. Pfflner and L. Guzzella, "Optimal operation of cvt-based powertrains," *Int. J. Robust Nonlinear Control*, vol. 11, no. 11, pp. 1003–1021, 2001.
 - [35] M. Coleman, W. G. Hurley, and C. K. Lee, "An improved battery characterization method using a two-pulse load test," *IEEE Transactions on Energy Conversion*, vol. 23, no. 2, pp. 708–713, 2008.
 - [36] R. Rao, S. Virudhula, and D. Rakhmatov, "Battery models for energy aware system design," *IEEE Computer*, vol. 36, pp. 1019–1030, 2003.
 - [37] V. Agarwal, K. Uthaichana, R. DeCarlo, and L. H. Tsoukalas, "Development and validation of a battery model useful for discharging and charging power control and lifetime estimation," *IEEE Transactions on Energy Conversion*, vol. 25, pp. 821–835, August 2010.
 - [38] S. Pekarek, K. Uthaichana, S. Benghea, R. DeCarlo, and M. Žefran, "Modeling of an electric drive for a hev supervisory level power flow control problem," in *2005 IEEE Vehicle Power and Propulsion Conference*, (IEEE Cat. No.05EX1117C), (Chicago, IL, USA), IEEE, 2005.
 - [39] M. Anatone, R. Cipollone, and A. Sciarretta, "Control-oriented modeling and fuel optimal control of a series hybrid bus," in *SAE Technical Papers 2005-01-1163*, 2005.
 - [40] S.-I. Jeon, S.-T. Jo, Y.-I. Park, and J.-M. Lee, "Multi-mode driving control of a parallel hybrid electric vehicle using driving pattern recognition," *Journal of Dynamic Systems, Measurement and Control, Transactions of the ASME*, vol. 124, no. 1, pp. 141–149, 2002.
 - [41] M. Koot, J. T. B. A. Kessels, B. de Jager, W. P. M. H. Heemels, P. P. J. van den Bosch, and M. Steinbuch, "Energy management strategies for vehicular electric power systems," *IEEE Transactions on Vehicular Technology*, vol. 54, no. 3, pp. 771–82, 2005.
 - [42] J. Heywood, *Internal Combustion Engine Fundamentals*. McGraw-Hill, 1988.
 - [43] A. Giua, C. Seatzu, and C. Van Der Mee, "Optimal control of switched autonomous linear systems," in *Proceedings of the IEEE Conference on Decision and Control*, vol. 3, (Orlando, FL), pp. 2472–77, Institute of Electrical and Electronics Engineers Inc., 2001.
 - [44] S. Hedlund and A. Rantzer, "Optimal control of hybrid systems," in *Proceedings of the IEEE Conference on Decision and Control*, vol. 4, (Phoenix, AZ, USA), pp. 3972–77, IEEE, Piscataway, NJ, USA, 1999.
 - [45] S. Wei, K. Uthaichana, M. Žefran, R. A. DeCarlo, and S. Benghea, "Applications of numerical optimal control to nonlinear hybrid systems," *Nonlinear Analysis: Hybrid Systems*, vol. 1, no. 2, pp. 264–279, 2007.
 - [46] Z. K. Nagy and F. Allgöwer, "Nonlinear model predictive control: From chemical industry to microelectronics," in *Proceedings of the IEEE Conference on Decision and Control*, vol. 4 of *2004 43rd IEEE Conference on Decision and Control (CDC)*, (Nassau), pp. 4249–4254, 2004.